https://doi.org/10.1016/j.ijleo.2019.163552

Performance assessment of GNSS scalar and vector frequency tracking loops

Jie Dou [1], Bing Xu [2] and Lei Dou [1,*]

[1] School of National Key Laboratory of Transient Physics, Nanjing University of Science and Technology, Nanjing 210094, China; doujienjust@163.com (J.D.)
[2] Interdisciplinary Division of Aeronautical and Aviation Engineering, The Hong Kong Polytechnic University, Kowloon, Hong Kong, China; pbing.xu@polyu.edu.hk (B.X.)
***** Correspondence: douleijs@163.com

Received: date; Accepted: date; Published: date

Abstract: This paper focuses on two types of frequency lock loops (FLL) in Global Navigation Satellite System (GNSS) receivers, namely the conventional scalar frequency lock loop (SFLL) and the vector frequency lock loop (VFLL).The VFLL has been proven to have a better tracking performance than the SFLL in scenarios such as intermittent signal outages, high dynamics, etc.. However, the FLL tracking performance under the equivalent noise bandwidth has not been explored in literature. To do this, we implemented three kinds of FLL, i.e., the SFLL, the weighted least square-based vector frequency loop (WLS-VFLL), and the extended Kalman filter-based vector tracking loop (EKF-VFLL). All these FLLs have the same noise bandwidth, based on which we made a fair comparison between them. The experimental static data and simulated high- dynamic data have been tested. Results show that the EKF-VFLL has a similar tracking performance with WLS-VFLL under static environment, both better than the SFLL. In high- dynamic environment, the advantages of EKF-VFLL are more prominent than the other two methods. Furthermore, EKF-VFLL takes the longest time in terms of computational efficiency.

Keywords: global navigation satellite system (GNSS); Extended Kalman filter (EKF); weighted least square (WLS); frequency lock loop (FLL); equivalent noise bandwidth

---

1. Introduction

In the global navigation satellite system (GNSS) field, receivers' signal tracking process is actually an estimation process for carrier frequency and the pseudo-random noise (PRN) code phase. For carrier tracking, the traditional scalar frequency lock loop (SFLL), is widely used. The SFLL can deal with moderate high dynamics. However, in some severe scenarios like huge dynamics and weak signals, it is incapable of action. To solve those problems, the concept vector tracking loop (VTL) was proposed in [1]. Generally, the extend Kalman filter (EKF) is used in the vector tracking loop architecture as the navigation estimator, referred to as EKF-VTL in this paper. In the SFLL, each channel tracks only one satellite, therefore the tracking architecture is simple and easy to implement. Unlike the SFLL architecture, the VTL combines the tracking loops and the navigation solving together using a single Kalman filter [2], taking full advantage of internal links between each tracking channels.

The advantages of VTL against the STL have been extensively exploited by many scholars [3,4]. Existing researches have shown that vector frequency lock loop (VFLL) has a better tracking performance in many harsh scenarios, such as high dynamics, low carrier-to-noise ratio (CNR), intermittent signal outages and multipath [5–8]. In [5], Lashley and Bevly reviewed the vector delay/frequency lock loop (VDFLL) and made a comparative analysis with the scalar tracking loop. The work in [9] demonstrated that VFLL can provide more reliable Doppler measurements and make the satellite signal easy to track by using an ultra-tightly couple (UTC) receiver. Furthermore, some analyses of the VFLL are carried out by [10] in terms of the robustness of the VFLL in different experimental conditions through a software defined GPS receiver, achieving a better tracking accuracy even when the signal is getting weaker.

However, those comparisons neglected the fact that, unlike the fixed noise bandwidth in STL, the VTL has different noise bandwidths for each channels [11]. For EKF-based VFLL, the bandwidth of each channel is adaptively adjusted according to the receiver dynamics. In addition, to the best of the authors' knowledge, the comparison of computation load for those two methods is rarely found in existing literatures.

In response to the above two limitations, we draw on Bhattacharyya's argument in terms of the noise bandwidth of the VTL [11] and use it to adjust the noise statistics of EKF-VFLL to the same level as SFLL. As mentioned earlier, since the noise bandwidth has a great influence on tracking performance and it was ignored by the existing researches. A larger loop bandwidth is needed for high-dynamic applications, but will introduce more noise, resulting in lower tracking precision. On the contrary, a smaller loop bandwidth should be considered to ruduce the noise level and improve the tracking accuracy. Therefore, it is necessary to comapre the STL and VTL on the common ground. Specifically, a weighted least square based vector frequency lock loop (WLS-VFLL) is considered, which has the same noise bandwidth statistics with that in FLL. Besides, the computational efficiency needs to be taken into account in some special applications. To determine the efficiency of SFLL and VFLL operation, we use the same signal length and simulate the tracking process over several Monte-Carlo (MC) runs.

With the purpose of making a fair comparison between SFLL and VFLL, in this paper, the equivalent noise bandwidth was expected to bring them into alignment. Firstly, the structure and principle of the FLL, WLS-VFLL and EKF-VFLL are compared for GNSS application. Secondly, the high dynamic GPS L1-like signals are generated and the field static signals are collected to assess those three methods. Finally, the frequency tracking deviation of the signals and the Central Processing Unit (CPU) times are presented for a more overall analysis of performance. The contributions of this paper could be summarized as:

(1) We make a fair comparison between the SFLL and VFLL, in which the equivalent noise bandwidth and computation time are taken into consideration, different from the existing experimental comparisons.

(2) Comparative analyses are implemented in terms of tracking accuracy and efficiency, which provide reasonable reference for the future research of VTL and develop a comprehensive understanding of why VFLL achieves a better tracking performance than SFLL.

The rest of the paper is organized as follows. The methodology of the assist each other channels during the VTL and the relationship with STL are introduced in section “Superiority of the VTL”. Frequency lock loop error sources and equivalent comparison conditions are reviewed in the section “Characteristic analysis” and the equivalent noise bandwidth calculation is detailed described in the section “Noise bandwidths analysis”. The section “Results and analysis” shows the comparison results under low CNR signal and high dynamic situations and the analysis is provided. Finally, “Conclusions” concludes the paper, including future work.

2. Superiority of the VTL

The architecture and implementation of the VTL and STL are illustrated in this section. In addition, the reason why the vector-based method outperforms scalar tracking loop is analyzed in detail. To make a comparison between the STL and VTL, both the similarity and the difference of them are also described.

2.1. Architecture

As shown in Figure 1, the tracking processes in different channels are independent of each other in the STL. The feedbacks driving the carrier and code NCOs are obtained from the discriminators directly. It is obviously that there is no information shared between channels in the STL. But for VTL, by making the most of the internal connections between the tracking channels, VTL couples all the channels information together using a single navigation processor. Based on the navigation solutions and the satellite ephemeris, the navigation processor can predict the receiver states information including position, velocity, clock bias and drift. In specific, the code phase errors and the frequency errors that obtained from the discriminator output are not used to correct the corresponding NCO directly. The discriminator outputs are converted to pseudo-range error and pseudo-range rate error measurements. With the navigation solution and satellite ephemeris, the code and frequency errors at next epoch can be predicted to drive the NCO. If only use the pseudoranges information in the state formulation of EKF, the vectorized method is called VDLL. Furthermore, both pseudoranges and pseudoranges rate can be used to establish the VDFLL.

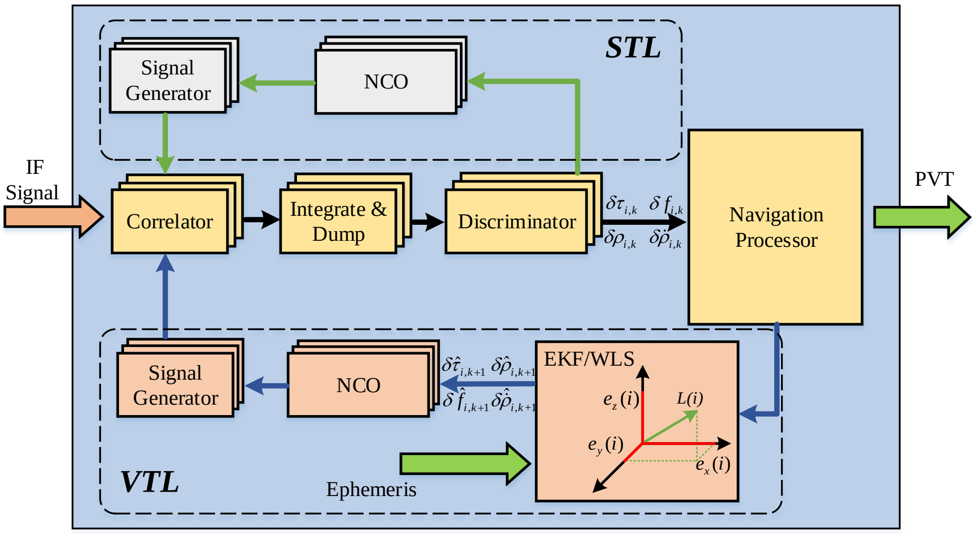

Fig. 1. Block diagram of the STL and VTL.

2.2. EKF-based tracking loop

In this paper, the comparison between the VFLL and the SFLL is made, and the extended Kalman filter (EKF) model and method is used in the integration unit. The EKF consists of two steps, i.e., prediction and correction. First of all, the state vector and covariance is initialized, on the left of the picture 1, the state vector is predicted by the measurements after correction and the estimation uncertainty is updated according to the process noise. In the correction stage, the Kalman gain matrix is updated for the purpose of making the state estimation optimal. The covariance matrix of estimation error is updated based on the new information from the measurements.

In the VTL, the EKF estimates the receiver states of position, velocity and time (PVT) through its system integration and measurements. After that, the pseudorange and its rate and the line-of-sight (LOS) vector between the satellites and the receiver are obtained from the ephemeris, which is known as a priori information. Finally, carrier NCOs are formed with the predicted pseudorange rates, for adjusting the frequency of local carrier replica in each channel.

The state vector of EKF is presented as:

$$\boldsymbol{X} = \begin{bmatrix} \delta v_x & \delta v_y & \delta v_z & \delta \dot{t} \end{bmatrix}^T \tag{1}$$

where δv_x , δv_y and δv_z are the three dimensional receiver velocity errors in an earth-centered and earth-fixed (ECEF) coordinates; $\delta \dot{t}$ is the receiver clock drift error. The system state equation at epoch k is as follows:

$$\hat{\boldsymbol{X}}_k = \boldsymbol{\Phi}_{k-1} \hat{\boldsymbol{X}}_{k-1} \tag{2}$$

where

$$\boldsymbol{\Phi}_{k-1} = \boldsymbol{I}_{4\times 4} \tag{3}$$

Here assumed that there are n visible satellites. The measurement of EKF is pseudorange rate error which is the difference between the measured values and the predicted ones. The pseudo- range rate error of satellite j is as follows:

$$\delta\dot{\rho}_j = f^j_{\text{Doppler}} \cdot \frac{c}{f_{\text{L1}}} - \left(\boldsymbol{v}_{\text{u}} - \boldsymbol{v}^j_{\text{s}}\right) \cdot \boldsymbol{l}^j - \hat{t}_{\text{u}} + t^j_{\text{s}} \tag{4}$$

where f^j_{Doppler} is the Doppler shift frequency in Hz; f_{L1} is the carrier frequency; $\boldsymbol{v}_{\text{u}}$ and $\boldsymbol{v}^j_{\text{s}}$ are the velocity vector of the receiver and satellite j, respectively; $\boldsymbol{l}^j$ is the LOS unit vector form the receiver to satellite j; $\hat{t}_{\text{u}}$ and t^j_{s} are the estimated receiver clock drift and the satellite clock drift, respectively. The measurement vector of EKF-VFLL can be presented by:

$$\boldsymbol{Z} = \begin{bmatrix} \delta\dot{\rho}_1 & \delta\dot{\rho}_2 & \cdots & \delta\dot{\rho}_{\text{n}} \end{bmatrix} \tag{5}$$

The measurement equation is the function of the state vector with a first-order Taylor's expression, which is given by:

$$\boldsymbol{Z}_k = \boldsymbol{H}_k \cdot \boldsymbol{X}_k \tag{6}$$

where $\boldsymbol{H}$ is the measurement matrix, calculated by

$$\boldsymbol{H} = \begin{bmatrix} e_{1,x} & e_{1,y} & e_{1,z} & 1 \\ e_{2,x} & e_{2,y} & e_{1,z} & 1 \\ \vdots & \vdots & \vdots & \vdots \\ e_{n,x} & e_{n,y} & e_{1,z} & 1 \end{bmatrix} \tag{7}$$

According to literature [12,13], the discrete time process noise covariance matrix can be divided into user dynamic noise and receiver clock noise, as shown in Equation (8).

$$\boldsymbol{Q} = \boldsymbol{Q}_{clk} + \boldsymbol{Q}_{dyn} \tag{8}$$

where the process noise covariance matrix due to the clock noise is drawn by:

$$\boldsymbol{Q}_{clk} = \begin{bmatrix} q_c & \cdots & q_c \\ \vdots & \ddots & \vdots \\ q_c & \cdots & q_c \end{bmatrix} \tag{9}$$

$$\boldsymbol{q}_c = \left[\sigma_d^2 T^3 / 3 \quad \sigma_d^2 T^2 / 2; \quad \sigma_d^2 T^2 / 2 \quad \sigma_d^2 \right] \tag{10}$$

The process noise covariance matrix due to the receiver dynamic is given by:

$$\boldsymbol{Q}_{dyn} = \begin{bmatrix} q_{1,1}^d & q_{1,2}^d & \cdots & q_{1,n}^d \\ q_{2,1}^d & q_{2,2}^d & \cdots & q_{2,n}^d \\ \vdots & \vdots & \ddots & \vdots \\ q_{n,1}^d & q_{n,2}^d & \cdots & q_{n,n}^d \end{bmatrix} \tag{11}$$

$$\boldsymbol{q}_{i,j}^d = \left[E_{i,j} T^3 / 3 \quad E_{i,j} T^2 / 2; \quad E_{i,j} T^2 / 2 \quad E_{i,j} T \right] \tag{12}$$

$$\boldsymbol{E}_{i,j} = e_x^i e_x^j \sigma_x^2 + e_y^i e_y^j \sigma_y^2 + e_z^i e_z^j \sigma_z^2 \tag{13}$$

As shown in equation (8), (9) and (10), both the clock noise and the dynamic state affect the noise covariance. As discussed earlier, VTL coupled all the channels together for the tracking performance enhancement. In particularly, because of the noise covariance is an off-diagonal matrix, the measured pseudo-range rate error obtained from one channel would affect the others. In other words, the signals are coupled together through the nonzero off-diagonal elements. The VTL can be converted to STL if makes the noise covariance matrix off-diagonal elements zeros.

The measurement noise covariance matrix is determined by the innovation-based adaptive estimation method. For detailed information, readers are referred to [14].

2.3. WLS-based tracking loop

As mentioned earlier, the superior performance of VFLL benefits from the Kalman filter, refer to the self-adjusted noise bandwidth. In order to guarantee the fair of comparison, here we use the WLS estimator to predict the user positioning, velocity, and time (PVT) information. The noise bandwidth of WLS-VFLL is fixed to the same with SFLL.

The state equations of three-dimensional velocity errors and clock drift errors in WLS-VTL is given by

$$\Delta\hat{\boldsymbol{v}} = \left(\boldsymbol{G}^T\boldsymbol{C}\boldsymbol{G}\right)^{-1}\boldsymbol{G}^T\boldsymbol{C}\boldsymbol{b} \tag{14}$$

$$\boldsymbol{b} = \begin{bmatrix} -\lambda f_d^{(1)} & -\lambda f_d^{(2)} & \cdots & -\lambda f_d^{(n)} \end{bmatrix}^T \tag{15}$$

where $\boldsymbol{G}$ is equivalent to $\boldsymbol{H}$ in the formula (1); $\boldsymbol{C}$ denotes the weighted matrix; $\boldsymbol{b}$ represents vector of pseudo-range rate error, obtained by the carrier Doppler shift measurements; λ is signal carrier wave length, $f_d^{(i)}$ is the Doppler shift measurement.

Furthermore, $\boldsymbol{C} = \boldsymbol{W}^{\mathrm{T}}\boldsymbol{W}$, W denotes n dimension diagonal matrix:

$$\boldsymbol{W} = \begin{bmatrix} w_1 & & & \\ & w_2 & & \\ & & \ddots & \\ & & & w_n \end{bmatrix} \tag{16}$$

where $w_n = 1/\sigma_n$, σ_n is the standard deviation of Doppler shift measurement error [15]. For a SFLL, the main sources of the Doppler tracking errors consist of thermal noise and dynamic stress error, which will be separately introduced in next section.

So, the predicted three-dimensional velocity can be given by

$$\hat{\boldsymbol{v}}_u = \begin{bmatrix} \hat{v}_x \\ \hat{v}_y \\ \hat{v}_z \\ \delta\hat{\dot{t}} \end{bmatrix} = \begin{bmatrix} \hat{v}_{x,0} \\ \hat{v}_{y,0} \\ \hat{v}_{z,0} \\ \delta\dot{t}_0 \end{bmatrix} + \Delta\hat{\boldsymbol{v}} \tag{17}$$

Because the noise term in pseudo-range rate measurement is ignored, the pseudo-range rate measurement can be given by

$$\dot{\rho}^{(i)} = \dot{r}^{(i)} + \delta f_u - \delta f_s^{(i)} \tag{18}$$

where δf_u and $\delta f_s^{(i)}$ are receiver clock shift and satellite clock shift, respectively; $\dot{r}^{(i)}$ is the rate of geometric distance change between user receiver and *i*th satellite, which can be written as

$$\dot{r}^{(i)} = \left(\boldsymbol{v}_u - \boldsymbol{v}_s^{(i)}\right) \cdot \boldsymbol{l}^{(i)} \tag{19}$$

where $\boldsymbol{v}_u$ is the velocity of the user receiver; $\boldsymbol{v}_s^{(i)}$ is the velocity of satellite *i*; $\boldsymbol{l}^{(i)}$ is the line of sight (LOS) unit vector from receiver to satellite *i*. Combine equations (16), equations (18) and equations (19), the Doppler frequency estimation can be given as

$$\hat{f}_d^{(i)} = -\frac{\left(\left(\boldsymbol{v}_u - \boldsymbol{v}_s^{(i)}\right) \cdot \boldsymbol{l}^{(i)}\right) + \delta f_s^{(i)} \times f_c}{c} \tag{20}$$

where c is the speed of light; f_c is the carrier frequency.

Finally, the carrier NCO updating as

$$\hat{f}_{c,nco}^{(i)} = f_{IF} + \hat{f}_d^{(i)} + \delta \hat{f}_e \tag{21}$$

where f_{IF} and $\delta \hat{f}_e$ are the intermediate frequency and the carrier frequency error estimation, respectively.

Both the VFLL and SFLL are used to track the frequency error within the loops. The superiority of the VFLL is illustrated in the earlier sections. Even so, STL is still must to be mentioned, as it is a very development technology and is widely used in many traditional receivers. Furthermore, the tracking information like pseudo-ranges rate that obtained from the STL is required to initialize VFLL before the integration filter worked [16]. One more thing, for a long time at the beginning, the tracking error of the VTL is larger than STL due to the noise variance correction process [13].

3. Characteristic analysis

Before the comparison, the equivalent conditions of VFLL and SFLL have to be determined. In this paper, the same coherent integration times, CNR, and tracking threshold are used to make the comparison reasonable. Besides, another condition that has to be taken into consideration is the equivalent noise bandwidths. Because the noise bandwidth is a significant parameter of GNSS receiver design and the loop noise performance assessment, which indicates the ability of the loop to suppress noise. Large noise bandwidth allows the loop to deal with large dynamic, while smaller bandwidth can achieve a better tracking precision [17]. Equivalent noise bandwidth is the premise of a fair comparison. In this section, the frequency measurement errors and the tracking threshold are introduced briefly; the noise bandwidths of both VFLL and SFLL are illustrated and analyzed in detail.

3.1. Measurement errors

Frequency measurement errors include frequency jitter error and dynamic stress error. The thermal noise is treated as the only source of frequency tracking error because of the vibration- induced and the Allan deviation are too small to consider for a short coherent integration time [18]. Hence, thermal noise and dynamic stress error are the dominant error sources for SFLL.

In an SFLL, the 1-sigma frequency jitter due to thermal noise is [18]:

$$\sigma_{tFLL} = \frac{1}{2\pi T}\sqrt{\frac{4FB_n}{SNR}\left(1+\frac{1}{T\cdot SNR}\right)}\text{(Hz)} \tag{22}$$

where $F=1$ at high CNR; $F=2$ near threshold; $T=10$ is the integration and dump time; B_n is the noise bandwidth (Hz). In this paper, an integration time of 10 ms is used.

Because the EKF used the position, velocity, and acceleration information, which provide VFLL the ability to tack step and ramp changes in velocity with zeros steady-state error. While fail to track a ramp change in acceleration with zero steady-state error. According to the analysis from literature [3], only a second-order SFLL has comparable capabilities compare with VFLL. For this reason, this paper focuses on the second-order

SFLL and VFLL. The frequency measurement error accused by dynamic stress error can be calculated as [18]:

$$f_e = F_J \frac{f_{L1}}{c} (\frac{0.53}{B_n})^2 \tag{23}$$

where $F_J = \text{Jerk dynamic } (\text{m/s}^3)$.

From equation (22) and (23), the second-order SFLL is capable of a larger dynamic stress with the noise bandwidth increases, but this will causes a lot of noise to be brought in.

3.2. Tracking Threshold

Assuming that the receive signals are already acquired. While the tracking threshold determines whether or not the captured signals can be tracked. If the SFLL discriminator outputs exceed the threshold, the frequency tracking loops lose the lock. The tracking threshold is the first guarantee for providing a fair comparison. Therefore, the same tracking threshold is required in this paper. Rule of thumb tracking thresholds are used to analyze the tracking performance of VFLL and SFLL, which shown as [18]:

$$3\sigma_{FLL} = 3\sigma_{tFLL} + f_e \le 1/4T \ \ (\text{Hz}) \tag{24}$$

According to Equation (24), assuming the noise bandwidth and the CNR are determined, the maximum dynamics stress can be determined if the largest SFLL discriminator outputs does not exceed the tracking threshold. Furthermore, the increase in both thermal noise and dynamic stress error may result in loop unlocking. Thus, the programmable design of the noise bandwidth determines the characteristics of the SFLL in response to signal dynamic and noise statics.

4. Noise bandwidths analysis

As mentioned above, the noise bandwidth plays a key role in both accuracy and dynamic performances. Noise bandwidth is an excellent tool to suppress the input noise. Actually, both SFLL and VFLL can be seen as a closed-loop control system. For a second-order SFLL, the noise bandwidths can be derived from its transfer function model, if the damping ration and the nature frequency are known. However, it is more complicated for a VFLL. The parameters in the EKF are time varying, and the transfer function is closely related to the number of visible satellites, CNR, and line of sight (LOS) geometry. The noise bandwidths formulas will be derived in this section.

4.1. Design of SFLL

As shown in Figure 2, SFLL consists of frequency discriminator, loop filter, and carrier NCO. Here the four-quadrant arctangent discriminator is applied in SFLL to obtain the difference of frequency between the local carrier replica and the incoming carrier, expressed as

$$w_f = \frac{\mathrm{a\tan2}(\mathrm{P_{cross}}, \mathrm{P_{dot}})}{\mathrm{t_2} - \mathrm{t_1}} \tag{25}$$

where $\mathrm{P_{dot}} = \mathrm{I_{P1}} \times \mathrm{I_{P2}} + \mathrm{Q_{P1}} \times \mathrm{Q_{P2}}$, $\mathrm{P_{cross}} = \mathrm{I_{P1}} \times \mathrm{Q_{P2}} - \mathrm{I_{P2}} \times \mathrm{Q_{P1}}$, $\mathrm{I_{P1}}$ and $\mathrm{Q_{P1}}$ are the prompt in-phase (I) and quadrate-phase (Q) outputs of the integrated and dumped correlation process at epoch $\mathrm{t_1}$; $\mathrm{I_{P2}}$ and $\mathrm{Q_{P2}}$ are the outputs at next epoch $\mathrm{t_2}$.

After being filtered by the loop filter, the frequency errors are used to control the frequency of the NCO.

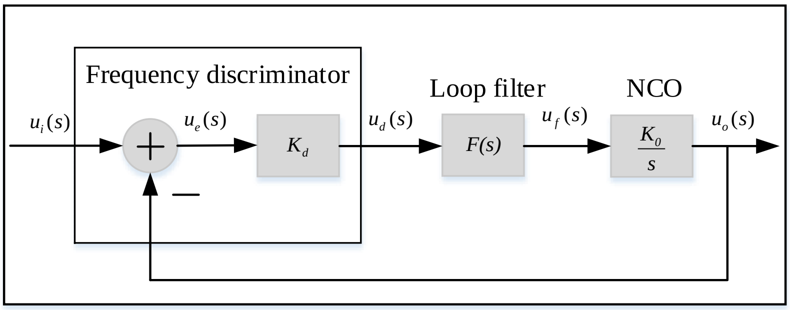

Fig. 2. Block diagram of SFLL in Laplace transforms.

According to Figure 2, the transfer function of SFLL can be express as the following equation [18]:

$$H(s)=\frac{u_{o}(s)}{u_{i}(s)}=\frac{K_{o}K_{d}F(s)}{s+K_{o}K_{d}F(s)}=\frac{KF(s)}{s+KF(s)} \tag{26}$$

where, $F(s)$ is the transfer function of loop filter, K_{o} and K_{d} are the gain of NCO and discriminator.

The discrete time system of a second-order SFLL is shown in Figure 3. In which, the parameters are key factors to make the system keep good performance, and the determination of the parameters can be reference literature [18].

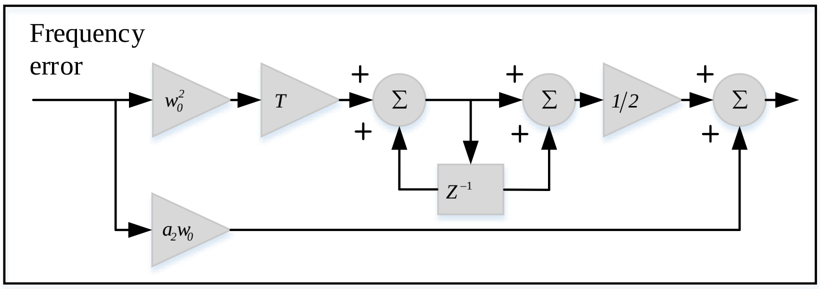

Fig. 3. Block diagram of FLL in discrete time system.

The transfer functions of filter loops of a second-order SFLL can be expressed as [18]:

$$F(s)=2\xi\omega_{0}+\frac{\omega_{0}}{s} \tag{27}$$

According to Equation (26), the transfer functions can be expressed as:

$$H(s)=\frac{2\xi\omega_{0}s+\omega_{0}^{2}}{s^{2}+2\xi\omega_{0}s+\omega_{0}^{2}} \tag{28}$$

From mentioned above, the noise bandwidth can be derived from the transfer functions, according to (26), the noise bandwidth of SFLL can be given by [18]:

$$B_{n}=\int_{0}^{\infty}\left|H_{s}(j2\pi f)\right|^{2}df=\frac{\omega_{0}}{2}(\xi+\frac{1}{4\xi}) \tag{29}$$

where, H_{s} is the frequency response function of a second-order SFLL. The damping ratio and noise bandwidth B_{n} both determine the frequency at the -3dB point.

4.2. Design of EKF-VFLL

Similarly, the noise bandwidth of the VFLL can be derived from the transfer function with a vector-based model. Assuming there are n satellites available, the prediction of the frequency in n channels can be expressed in vector $\hat{\boldsymbol{f}}_{k+1} = \left[\hat{f}_1^{k+1} \quad \cdots \quad \hat{f}_n^{k+1} \right]^T$, and the updated frequency is:

$$\hat{\boldsymbol{f}}_{k+1} = \hat{\boldsymbol{f}}_k + \Delta\hat{\boldsymbol{f}}_k \tag{30}$$

where, $\hat{\boldsymbol{f}}_k$ stands the frequency estimates at epoch k; $\Delta\hat{\boldsymbol{f}}_k$ is the frequency error estimation, and is used for carrier frequency correction at epoch k+1.

Because the frequency NCO is fed back to the local frequency generator, in which, the Doppler shift caused by user-satellite relative motion and the frequency residuals caused by the pseudo-range rate estimation errors are obtained. As for a VFLL, only the velocity term and the clock drift term are involved in EKF, therefore, the frequency NCO values can be calculated by [16]:

$$\Delta\hat{f} = \frac{f_{L1}}{c}\boldsymbol{E} \cdot \Delta\boldsymbol{V} \tag{31}$$

$$\boldsymbol{E} = \begin{bmatrix} e_x & e_y & e_z & -1 \end{bmatrix} \tag{32}$$

$$\Delta\boldsymbol{V} = \begin{bmatrix} \Delta\dot{v}_x & \Delta\dot{v}_y & \Delta\dot{v}_z & \Delta\dot{t} \end{bmatrix} \tag{33}$$

where, f_{L1} is the carrier frequency of GPS L1 (1575.42 MHz); c is the speed of the light; $\boldsymbol{E}$ stands the projection of user-satellite relative motion and clock error on LOS vector; $\Delta\boldsymbol{V}$ involves predictions of user-satellite relative velocity and clock drift at current epoch and estimation errors of next epoch. Hence, the formula (20) can be extended to [11]:

$$\Delta\hat{\boldsymbol{f}}_k = \frac{f_{L1}}{c}\boldsymbol{E}_k(\Delta\hat{\boldsymbol{V}}_k^r - \Delta\boldsymbol{V}_k^s) \tag{34}$$

where, $\Delta\boldsymbol{V}_k^s$ and $\Delta\hat{\boldsymbol{V}}_k^r$ are the correction terms of velocity and clock for satellite and user at epoch k+1, respectively. According to Kalman filtering theory, $\Delta\hat{\boldsymbol{V}}_k^r$ is updated in the EKF. Thus,

$$\begin{aligned}\Delta\hat{\boldsymbol{V}}_k^r &= \Delta\hat{\boldsymbol{V}}_{k-1}^r + \boldsymbol{K}_k(\Delta\boldsymbol{f}_k - \boldsymbol{E}_k\Delta\hat{\boldsymbol{V}}_{k-1}^r) \\ &= (\boldsymbol{I} - \boldsymbol{K}_k\boldsymbol{E}_k)\Delta\hat{\boldsymbol{V}}_{k-1}^r + \boldsymbol{K}_k\Delta\boldsymbol{f}\end{aligned} \tag{35}$$

where, $\boldsymbol{K}_k$ denotes the EKF gain matrix; $\Delta\boldsymbol{f}_k$, which is obtained by the frequency discriminator, is the carrier frequency residuals.

Combine formula (28) with formula (33), the updated frequency can be extended as:

$$\hat{\boldsymbol{f}}_{k+1} = \hat{\boldsymbol{f}}_k + \frac{\boldsymbol{E}_k}{\lambda_{L1}}\left[-\Delta\boldsymbol{V}_k^s + (\boldsymbol{I} - \boldsymbol{K}_k\boldsymbol{E}_k)\Delta\boldsymbol{V}_{k-1}^r + \boldsymbol{K}_k\Delta\boldsymbol{f}_k\right] \tag{36}$$

where, $\lambda_{L1} = c/f_{L1}$, stands for the wavelength of GPS L1 signal.

Because $\Delta\boldsymbol{V}_k^s$ and $\Delta\hat{\boldsymbol{V}}_{k-1}^r$ involved in EKF always remain constant during short carrier pre-detection time (e.g. 1ms), the performance of VFLL wouldn't be affected by these two terms. Thus, in order to simplify the algorithm, here these two terms are ignored. Then the simplified transfer function can be written as [11]:

$$\begin{aligned}\hat{\boldsymbol{f}}_{k+1} &= \hat{\boldsymbol{f}}_k + \frac{\boldsymbol{E}_k\boldsymbol{K}_k}{\lambda_{L1}}\Delta\boldsymbol{f}_k \\ &= \hat{\boldsymbol{f}}_k + \frac{\boldsymbol{E}_k\boldsymbol{K}_k}{\lambda_{L1}}(\boldsymbol{f}_k - \hat{\boldsymbol{f}}_k) \\ &= (\boldsymbol{I} - \frac{\boldsymbol{E}_k\boldsymbol{K}_k}{\lambda_{L1}})\hat{\boldsymbol{f}}_k + \frac{\boldsymbol{E}_k\boldsymbol{K}_k}{\lambda_{L1}}\boldsymbol{f}_k\end{aligned} \tag{37}$$

Taking the Laplace transform of (37), the transfer function can be written as:

$$\hat{\boldsymbol{f}}_{k+1}(s) = \boldsymbol{G}(s)\boldsymbol{f}_k(s) \tag{38}$$

$$\boldsymbol{G}(s) = (s\boldsymbol{I} + \frac{\boldsymbol{E}_k\boldsymbol{K}_k}{\lambda_{L1}})^{-1}\frac{\boldsymbol{E}_k\boldsymbol{K}_k}{\lambda_{L1}} \tag{39}$$

Because of $\boldsymbol{E}_k\boldsymbol{K}_k$ is an idempotent matrix. Hence,

$$\boldsymbol{E}_k\boldsymbol{K}_k = (\boldsymbol{E}_k\boldsymbol{K}_k)^2 = \cdots = (\boldsymbol{E}_k\boldsymbol{K}_k)^n \tag{40}$$

In addition, as discussed in literature [11], the transfer function model of a VFLL consists of $n \times n$ matrices, which expressed as:

$$\boldsymbol{G}(s)=\begin{bmatrix}\boldsymbol{G}_{1,1}(s) & \boldsymbol{G}_{1,2}(s) & \cdots & \boldsymbol{G}_{1,n}(s)\\ \boldsymbol{G}_{2,1}(s) & \boldsymbol{G}_{2,2}(s) & \cdots & \boldsymbol{G}_{2,n}(s)\\ \vdots & \vdots & \ddots & \vdots\\ \boldsymbol{G}_{n,1}(s) & \boldsymbol{G}_{n,2}(s) & \cdots & \boldsymbol{G}_{n,n}(s)\end{bmatrix} \tag{41}$$

In which, $\boldsymbol{G}_{i,q}(s)$ denotes the transfer function of the i^{th} row and the q^{th} column. According to equation (33), the corresponding noise bandwidth $\boldsymbol{B}_{VFLL}^{i,q}$ can be calculated. Because the geometric corrections of the channels are time varying, the noise bandwidth can be achieved from the diagonal noise bandwidth due to the empirical experience. So, According to the definition of noise bandwidth in literature [19], the noise bandwidth of VFLL can be derived as:

$$\begin{aligned}\boldsymbol{B}_{VFLL} &= \int_0^{\infty} \left|\boldsymbol{G}(f)\right|^2 df \approx \frac{\text{diag}(\boldsymbol{E}_k \boldsymbol{K}_k)}{2\lambda_{\text{L1}}\pi}\int_0^{\infty}\frac{1}{1+\omega^2 T^2}d\omega \\ &= \frac{\text{diag}(\boldsymbol{E}_k \boldsymbol{K}_k)}{4\lambda_{\text{L1}}T}\end{aligned} \tag{42}$$

It can be seen from the Equation (42); factors affecting noise bandwidth of VFLL include the number and geometry of visible satellites, carrier pre-detection time, and the EKF gain matrix. For example, the noise bandwidth is reduced by increasing the integral time, which means a good performance to suppress the input noise. And it is also illustrated that $\boldsymbol{B}_{VFLL}$ elements are adaptively changed according to user-satellite geometry and gain matrix. Because of the noise bandwidth characteristic of VFLL is more complicated than that in SFLL, so in conclusion, how to fairly compare the performance of VFLL and SFLL mainly depends on the selection of noise bandwidth. Because there is no single noise bandwidth for vector loops as the transfer function matrix shows that it is an interactive multi-input and multi-output system. So the noise bandwidth is defined with respect to an input channel. However, for comparing with a scalar loop the equivalent diagonal noise bandwidth of the vector loops may be considered as a reference.

5. Simulation and Results

To evaluate the frequency tracking performance of the SFLL and VFLL, the signals are processed on the same test bench, a software-defined receiver (SDR), which is based on the MATLAB platform [20]. The VFLL include EKF-VFLL and WLS-VFLL. In addition, the setting of parameters in the loop is also the same, such as tracking threshold, coherent integration time, frequency discriminators and equivalent noise bandwidth. In this paper, the coherent integration time is set as 10 milliseconds, frequency discriminator are obtained by Equation (20). Several noise bandwidths have been set to test the performance in different scenarios. The experimental data with different CNR and simulation data with extremely approximate CNR are also provided in this section. The 110-second experimental data of GPS L1 were collected in an open area in Hong Kong, with the equipment shown in Figure 4. The NovAtel antenna was mounted to the top of the automobile, which was used to receive the GPS L1 signals. In the first 30 seconds the car kept static and then moved with a moderate dynamic in the rest of the time. The Nottingham Scientific Ltd. (NSL) Stereo front-end was used to convert the radio frequency (RF) signals to intermediate frequency (IF) signal. The sampling frequency and the IF of the front-end are 26 MHz and 6.5 MHz, respectively.

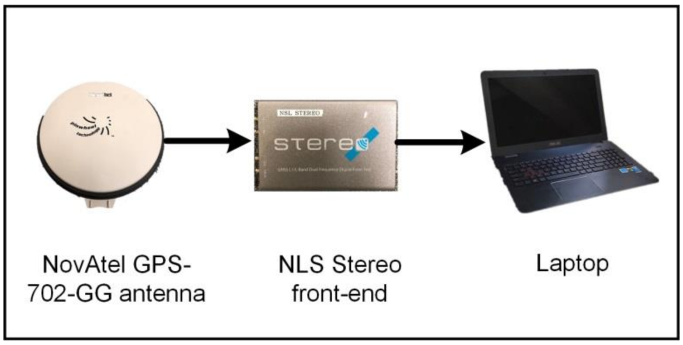

Fig. 4. Experimental setup.

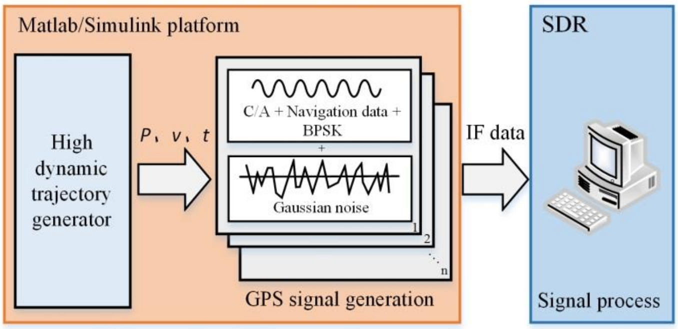

Fig. 5. The block diagram of simulation platform.

Because of the restrictions in experimental conditions, the GPS IF data in high dynamic environment is difficult to obtain. Here we use simulated signals to assess the frequency tracking performance of the SFLL and VFLL. As shown in Figure 5, the high-dynamic trajectory is firstly generated using the self-developed GPS IF signal simulator, which is based on the Matlab/Simulink platform. Then, IF GPS data is simulated by the GPS signal generator module. Finally, the IF data is input into the software-defined receiver module for the tracking experiments. The advantage of using simulated data is that the CNR is exactly controllable, and the signal characteristics are exactly known, which avoids the impact such as the ionospheric delay and multipath interference. Based on these conditions, the comparison of VFLL and SFLL are performed.

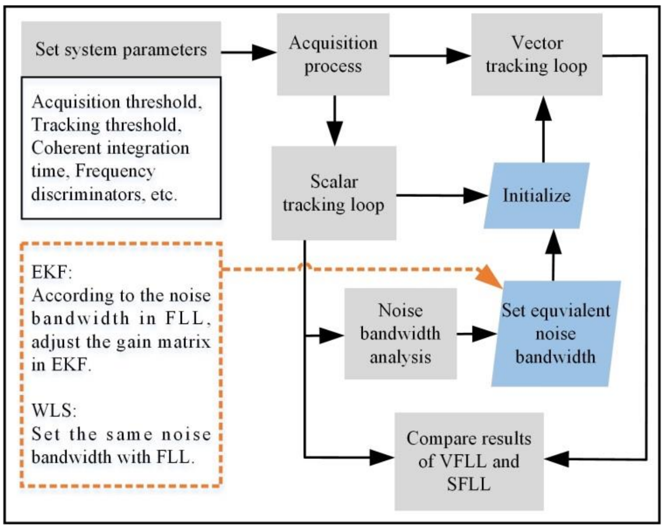

Fig. 6. The system architecture of the comparison.

Figure 6 shows the system architecture of the comparison operation. First, set the system parameters, such as acquisition threshold, tracking threshold, and coherent integration time, etc. Next, the signal acquisition is carried out to process the same data, in which the number of visible satellites used to track for the loop is determined. Following that, the SDR starts scalar tracking first, then the tracking results are used to initialize the vector tracking loop. Meanwhile, from the noise bandwidth analysis in section 4, to set the equivalent bandwidth, only the LOS matrix and Kalman gain matrix need to be adjusted. So the noise bandwidth of the SFLL is analyzed, and the equivalent noise bandwidth for VFLL is set so as to achieve the purpose of making a fair comparison. Finally, the tracking results of the VFLL and SFLL are provided, and the performance are analytical compared.

In particular, for the EKF-VFLL, the value of the corresponding gain matrix in the EKF is adjusted according to the bandwidth in SFLL. That is because the noise bandwidth of the EKF-VFLL loop is the function of gain and LOS vector matrix, as mentioned above, and the later component remain constant in a few second. For the WLS-VFLL, unlike the former, share the same noise bandwidth with SFLL.

5.1. Experimental results

Figure 7 shows the CNR of individual tracking channels during a period of 0-100 second. In this paper, CNR is estimated using the narrow-to-wide power ratio method [21]. As seen from the figure, there are seven satellites that have been tracked, with different CNR values. In the first 30 seconds, the CNR values of the tracking signals are relatively stable, between 35 and 55dB-Hz. Then the CNR varies due to the motion of the car. Especially in the last 30 seconds, the CNR of PRNs 12, 21 and 25 suffer a sudden drop due to the high dynamics of the car.

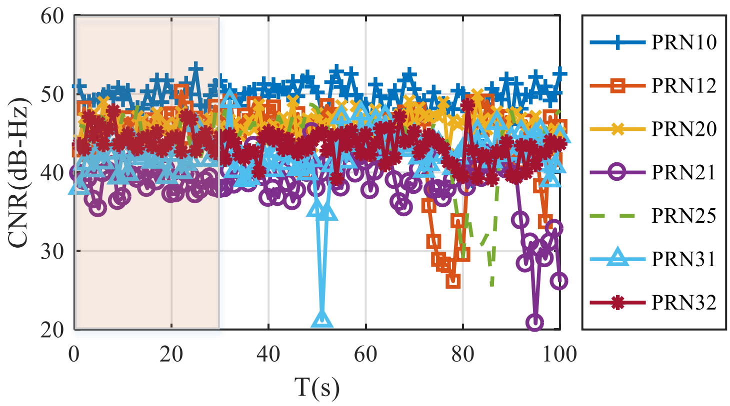

Fig. 7. Carrier-to-noise ratios of the tracking satellites.

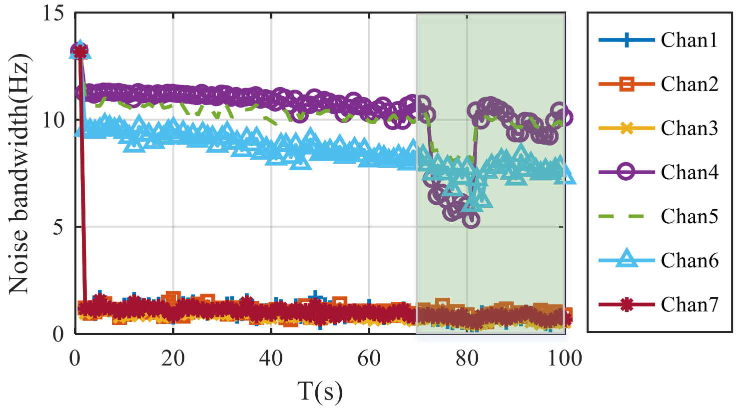

Fig. 8. Equivalent noise bandwidths of the EKF-VFLL.

Figure 8 shows the diagonal noise bandwidths of the VFLL, in which they are different from each other and time varying. The first channel in figure 6 corresponds to the PRN10 in figure 5, and so on. As we can see, the channel with high CNR (50dB-Hz) has a small noise bandwidth (0.58Hz). Hence, high CNR (PRN10) does not mean large noise bandwidth. That is because only EKF gain matrix and LOS vector matrix contribute to the noise bandwidth calculation. Any slight change in satellites geometry or measurement noise (accounts for the gain matrix) will result in bandwidth variation. As shown in the light green shadow, the CNR of PRNs 21, 25 and 31 decrease due to the automobile dynamics.

In order to assess the carrier frequency tracking performance of these three methods, the metric of frequency lock indicator (FLI) is used. The FLI is obtained by frequency errors and integration time [22]

$$\mathrm{FLI} \approx \cos(4\pi \cdot \delta f \cdot \mathrm{T}) \tag{43}$$

The values of the lock indicator range from -1 to 1, where larger value indicates smaller frequency error and 1 means perfect lock with zero Hz of frequency error. In this paper, the second order SFLL assisted third order PLL carrier tracking loop is carried out in STL, and the bandwidth of the SFLL and WLS-VFLL are 10Hz. For simplicity, just take channel 1 for example, the FLI results of SFLL, WLS-VFLL and EKF-VFLL are shown in Figure 9. Generally, the integration time is 10 ms, a FLI of 0.90 corresponds to only a few Hz of frequency error. It is obviously to find that, the frequency tracking errors of WLS-VFLL and EKF-VFLL are very close, both smaller than that in SFLL. This is due to that the tracking residuals in VFLL are more likely to be reduced by the information exchange between signals and the channels coupled together in the navigation processor. At around 75 s, the FLI of SFLL and VFLL suffer a sudden decrease, due to the automobile dynamics. About 5 s, the FLIs of VFLL are recover to the normal level, while for the SFLL, it takes more time.

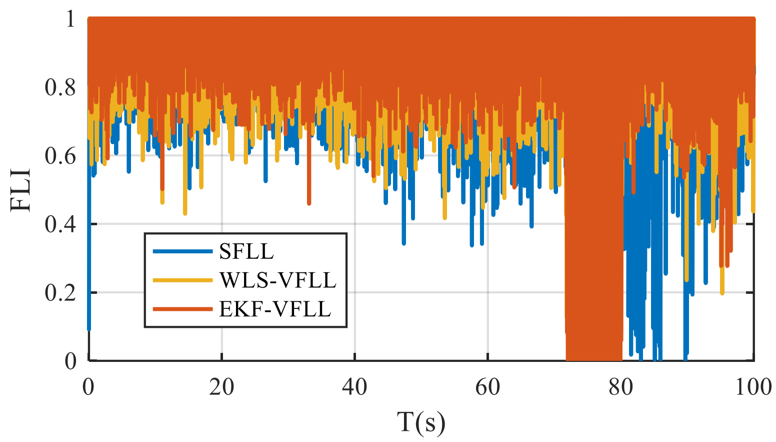

Fig. 9. Frequency lock indicator for FLL, WLS-VFLL and EKF-VFLL.

Table 1
RMS of frequency errors of different tracking strategies with the same noise bandwidth.

Methods	RMS of Frequency errors (Hz)		
	Without	**With 10Hz**	**With 15Hz**
SFLL	42.55	42.55	50.20
WLS-VFLL	26.75	28.75	33.45
EKF-VFLL	26.35	27.00	28.80

Again, takes channel 1 as an example, to test the tracking performance of VFLL and SFLL under the same bandwidth, set the VFLL bandwidth to 10Hz (equivalent with FLL) in Figure 4. For a short period of time, the geometry between the satellite and the receiver remains unchanged, thus, the LOS matrix can be viewed as being constant. According to Equation (37), set the gain matrix to corresponding values, so as to achieve the equivalent bandwidth. The detail tracking results comparison of the traditional SFLL, WLS-VFLL and EKF-VFLL is listed in Table 1. Interestingly, although the noise bandwidth in EKF-VFLL is increased, the tracking error is not huge raised, still close to WLS- VFLL, superior to SFLL on that equivalent noise bandwidth. However, the RMS of frequency errors in SFLL suffered a sharp rise as shown in Table 1. For the other tracking channels, we get the similar results, as shown in Figure 10.

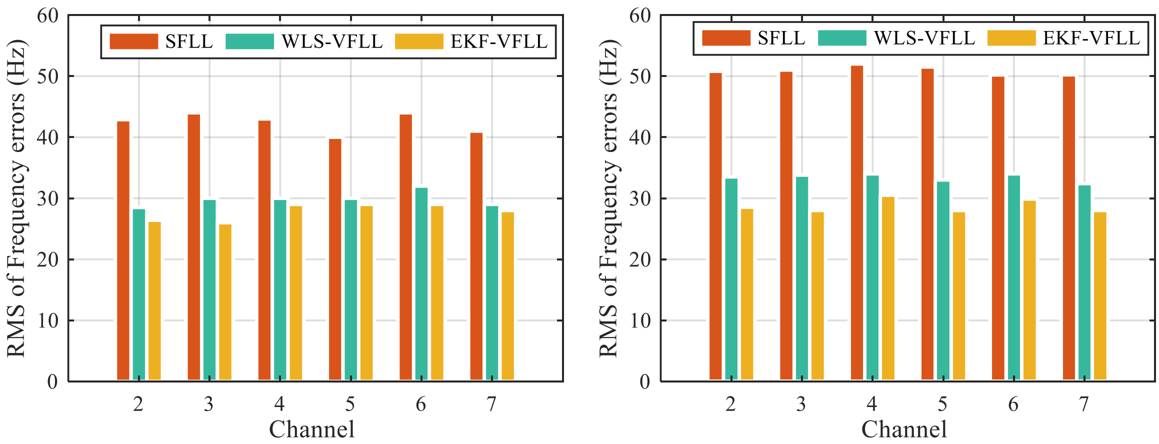

(a) (b)

Fig. 10. RMS of frequency errors under the same bandwidth. (a) 10 Hz; (b) 15 Hz.

It can be seen that SFLL is more sensitive to noise bandwidth; EKF-VFLL is almost immune to noise bandwidth. In addition, to demonstrate the computational loads of those three methods for real GPS signals, we use the MATLAB function tic-toc to find out how much time it costs for the tracking process. The computer simulation environment is as follows. The simulation software is MATLAB 2016b. We collected 10s IF signal. The CPU is Intel Core i5-6500 (3.20 GHz) and the memory is 8.00 GB RAM. The system environment is Windows 10 with 64 bits. Table 2 listed the computational loads of those three methods over 10 MC runs. SFLL has a faster tracking speed. Despite the performance of EKF-VFLL was superior, but it takes longer time than the other two methods. There are two reasons for this; one is prediction and correction steps, the other one is the complex matrix operations involved.

Table 2
Computational loads

Item	SFLL	WLS-VFLL	EKF-VFLL
Time (s)	225.00	318.50	390.02

5.2. Simulation results

In this section, the simulation results are carried out, in which the high dynamic scenario is taken into consideration. The 60s generated IF signals was used here, which is similar to real satellite signals. Because the superiority of VDLL have been proven in literature [5], when the number of the visible satellites exceed four. As a perfection to this, here just take into account that only four satellites available, and assumed that the satellites positions are exactly known as: $S_1(26,0,0)$, $S_2(0,0,-15)$, $S_3(0,0,15)$, $S_4(9,15,0)$, $S_5(-9,7,0)$; the unit is *km*. The coordinates of the vehicle are set at the origin. During the simulation, the maximum velocity is 1500m/s, the maximum acceleration is 25.5g, all satellites have the same CNR of 45 dB-Hz. The sampling frequency is 12MHz and the intermediate frequency 3.563MHz.

Figure 11 illustrates the noise bandwidth of each tracking channel in VFLL. With the motion of the vehicle, the bandwidth show a greatly fluctuates. Since the CNR of each channel is equivalent, the EKF gain matrix is fixed. The fluctuation is mainly caused by the change of the vehicle-satellite geometric in the process of motion. This can also be confirmed by channel 2 and channel 3; both of them have the same bandwidth, as they have the symmetrical geometric relative to the trajectory of the vehicle.

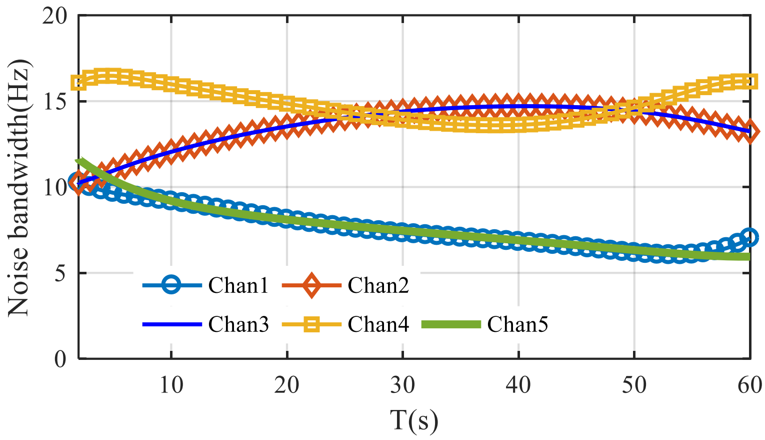

Fig. 11. Equivalent noise bandwidths of EKF-VFLL

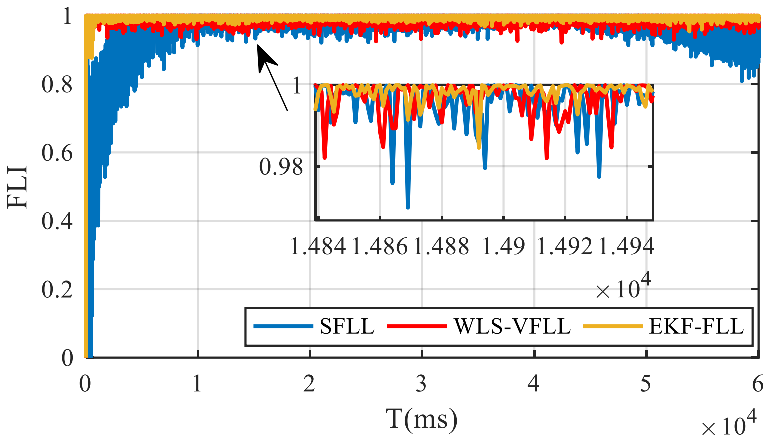

Fig. 12. FLI of SFLL, WLS-VFLL and EKF-VFLL under high dynamic scenario

The frequency tracking errors of VFLL and SFLL are shown in Figure 12. The bandwidth of the SFLL is set to 30Hz. Similar to the results in experimental operation; the EKF-VFLL has a better tracking performance than that in SFLL. However, the tracking performance in WLS-VFLL is worse than that in EKF-VFLL, under high dynamic scenario. This is due to its variable bandwidth in the EKF-based tracking loops, which has the ability to suppress the noise adaptively. In contrast, the bandwidth in WLS-based tracking loop is fixed.

In the process of simulation, it is interesting to find that, when set the SFLL bandwidth equal to that in EKF-VFLL, the improvement tracking results are achieved. However, although the tracking performance in SFLL is improved, it was still worse than that in WLS- and EKF-based VFLL. For a vector-based tracking loop, since it is a multi-input and multi-output system, all channel information is deeply integrated via the measurement matrix in EKF. Particularly, the information exchanges between signal tracking depend on non-diagonal element within the matrix. That explains why VFLL can achieve a better tracking performance although it has the same bandwidth with SFLL. Furthermore, the results above indicate that EKF-VFLL can achieve a better tracking performance under high dynamic scenarios due to its variable noise bandwidth. These methods employed with SFLL and WLS-VFLL is incapable of enduring this high dynamic environment and estimates the carrier Doppler optimally.

6. Conclusions

A fair comparison between SFLL, WLS-VFLL and EKF-VFLL has been proposed in this paper. It took equivalent bandwidth of VFLL into consider, which based on the function of LOS matrix and EKF gain. By bring the comparison conditions to one common ground, a fair comparisons has been made. Both experimental data with different signal quality and simulated data with the same Signal quality have been tested using a SDR.

Experimental results demonstrated that both EKF-VFLL and WLS-VFLL have a better tracking performance than traditional FLL under static environment. However, the EKF-based tracking loop has a bigger computation burden due to the complexity of filter structure, comparing with the other two methods. In addition, because EKF- VFLL is immune to the noise bandwidth, the tracking performance of EKF-VFLL is still superior to FLL, even if they have the same bandwidth.

Simulation results indicate that EKF-VFLL can achieve a higher tracking accuracy than WLS-VFLL and SFLL by its variable noise bandwidth, under high dynamic conditions. Since WLS-VFLL has the same bandwidth with SFLL, the performance of the method under high dynamic environment is a little better than that in SFLL, but worse than EKF-VFLL.

The method that used to reduce the computational load and simplify the filtering process will be studied in the future work.

Author Contributions: J.D. and L.D. conceived and designed the simulation; B.X. assisted to collect the real GPS signal data and revise the paper; J.D. drafted the manuscript.

Funding: This work was supported by National Natural Science Foundation of China (grant number 60904085); Foundation of National Key Laboratory of Transient Physics; and Foundation of Defence Technology Innovation Special Filed.

Conflicts of Interest: The authors declare no conflict of interest.

References

[1] S. Lim, D.W. Lim, M. Liu, S.W. Moon, C. Park, S.J. Lee, Design of a software-based multi-channel GNSS if signal generator, in: 2008 Int. Conf. Control. Autom. Syst. ICCAS 2008, 2008. doi:10.1109/ICCAS.2008.4694599.

[2] T. Pany, R. Kaniuth, B. Eissfeller, Deep integration of navigation solution and signal processing, Proc. ION-GNSS 2005, 13-16 Sept. 2005. (2005) 13–16. http://www.ion.org/search/view_abstract.cfm?jp=p&idno=6305%5Cnhttp://forschung.unibw-muenchen.de/ainfo.php?PHPSESSID=tkolzjca&id=6015.

[3] A. Shafaati, T. Lin, A. Broumandan, G. Lachapelle, Design and implementation of an RTK-based vector phase locked loop, Sensors (Switzerland). 18 (2018). doi:10.3390/s18030845.

[4] X. Chen, X. Wang, Y. Xu, Performance enhancement for a GPS vector-tracking loop utilizing an adaptive iterated extended kalman filter, Sensors (Switzerland). 14 (2014) 23630–23649. doi:10.3390/s141223630.

[5] M. Lashley, D.M. Bevly, J.Y. Hung, Performance analysis of vector tracking algorithms for weak GPS signals in high dynamics, IEEE J. Sel. Top. Signal Process. 3 (2009) 661–673. doi:10.1109/JSTSP.2009.2023341.

[6] M. Lashley, D.M. Bevly, Comparison in the Performance of the Vector Delay / Frequency Lock Loop and Equivalent Scalar Tracking Loops in Dense Foliage and Urban Canyon, Proc. 24th Int. Tech. Meet. Satell. Div. Inst. Navig. (ION GNSS 2011), 20-23 Sept. 2011. (2011) 1786–1803.

[7] S. Chen, Y. Gao, Improvement of carrier phase tracking in high dynamics conditions using an adaptive joint vector tracking architecture, GPS Solut. 23 (2019) 1–10. doi:10.1007/s10291-018-0806-y.

[8] D.J. Jwo, Z.M. Wen, Y.C. Lee, Vector tracking loop assisted by the neural network for GPS signal blockage, Appl. Math. Model. 39 (2015) 5949–5968. doi:10.1016/j.apm.2015.06.004.

[9] D. Sun, M.G. Petovello, M.E. Cannon, Ultratight GPS/reduced-IMU integration for land vehicle navigation, IEEE Trans. Aerosp. Electron. Syst. 49 (2013) 1781–1791. doi:10.1109/TAES.2013.6558019.

[10] T. Pany, B. Eissfeller, Use of a vector delay lock loop receiver for GNSS signal power analysis in bad signal conditions, in: Rec. - IEEE PLANS, Position Locat. Navig. Symp., 2006: pp. 893–903. doi:10.1109/PLANS.2006.1650689.

[11] S. Bhattacharyya, Vector Loop Transfer Functions and Noise Bandwidths, Navig. J. Inst. Navig. 65 (2018) 55–72. doi:10.1002/navi.219.

[12] M. Lashley, D.M. Bevly, J.Y. Hung, A valid comparison of vector and scalar tracking loops, Rec. - IEEE PLANS, Position Locat. Navig. Symp. (2010) 464–474. doi:10.1109/PLANS.2010.5507215.

[13] L.-T. Hsu, P.D. Groves, S.-S. Jan, Assessment of the Multipath Mitigation Effect of Vector Tracking in an Urban Environment, Proc. ION 2013 Pacific PNT Meet. Honolulu, Hawaii, April. (2013) 498–509.

[14] A.H. Mohamed, K.P. Schwarz, Adaptive Kalman filtering for INS/GPS, J. Geod. 73 (1999) 193–203. doi:10.1007/s001900050236.

[15] K. Krumvieda, C. Cloman, E. Olson, J. Thomas, W. Kober, P. Madhani, P. Axelrad, A complete IF software GPS receiver- A tutorial about the details, 14 Th Int. Tech. Meet. Satell. Div. Inst. Navig. GPS 2001), Salt Lake City, UT. (2001) 789–829.

[16] Z. Sun, X. Wang, S. Feng, H. Che, J. Zhang, Design of an adaptive GPS vector tracking loop with the detection and isolation of contaminated channels, GPS Solut. 21 (2017) 701–713. doi:10.1007/s10291-016-0558-5.

[17] L. Zhao, L. Shi, C. Zhu, New Nonlinear Second-Order Phase-Locked Loop with Adaptive Bandwidth Regulation, Electronics. 7 (2018) 346. doi:10.3390/electronics7120346.

[18] Kaplan Elloit;Hegarty Christopher, Understading GPS and applications, n.d.

[19] S. Bhattacharyya, D. Gebre-Egziabher, Development and validation of parametric models for vector tracking loops, Navig. J. Inst. Navig. 57 (2010) 275–295. doi:10.1002/j.2161-4296.2010.tb01783.x.

[20] B. Xu, L.T. Hsu, Open-source MATLAB code for GPS vector tracking on a software-defined receiver, GPS Solut. 23 (2019) 1–9. doi:10.1007/s10291-019-0839-x.

[21] P.D. Groves, GPS signal-to-noise measurement in weak signal and high-interference environments, Navig. J. Inst. Navig. 52 (2005) 83–94. doi:10.1002/j.2161-4296.2005.tb01734.x.

[22] C. Mongrédien, G. Lachapelle, M.E. Cannon, Testing GPS L5 Acquisition and Tracking Algorithms Using a Hardware Simulator, Engineering. (2008) 26–29.